

Thermal Analysis Kinetics of the Solid-State Reduction of Nickel Laterite Ores by Carbon

Xueming Lv, Xuewei Lv, Lunwei Wang and Jie Qiu

Abstract Non-isothermal multiple scanning rate analysis method was used to analyse the solid-state reduction of nickel laterite by carbon. According to the TG curves, the activation energies were calculated and the most probable mechanism functions were determined by the Malek method. The results show that the process can be divided into three stages according to the reaction degree (α): 0–40%, 40–70%, 70–100%, respectively. In the stage of $0 \leq \alpha \leq 0.40$, the most probable mechanism function fits the chemical reaction order function. In the stage of $0.40 \leq \alpha \leq 0.70$ and $0.70 \leq \alpha \leq 1.0$, the process may not be exactly described by one mechanism function.

Keywords Nickel laterite · Solid-state reduction · Thermal analysis kinetics · Activation energy

Introduction

Nickel sulfide ores and nickel laterite ores are the two main resources for extracting nickel metal. In recent years, there has been an increased focus on the utilization of low-grade nickel laterite ore, along with a growing demand for stainless steel and a declining supply of sulfide ores. Therefore, in the long term, it will be necessary to optimise nickel extraction from nickel laterite ore [1–5].

Several investigations of nickel laterite ore reduction have been performed. For example, Jankovic et al. studied reduction kinetics of nickel oxide with hydrogen under non-isothermal conditions, the activation energies were 96.4 kJ/mol, then the most probable mechanism function was determined to be $f(\alpha) = \alpha^{0.63}(1 - \alpha)^{1.39}$ [6, 7]. Jungah et al. studied reduction kinetics of nanocrystalline Fe_2O_3 –NiO by solid

X. Lv · X. Lv (✉) · L. Wang · J. Qiu
College of Materials Science and Engineering, Chongqing University,
Chongqing 400044, China
e-mail: lvxuewei@163.com

carbon and the results showed that reduction rate improved constantly with increasing temperature, the reduction rate was controlled by Boudouard reaction [8].

Since the previous study mainly confined to reduction of pure nickel oxide, there is a few study on reduction of nickel laterite ores and rarely used carbon as reducing agent. In this paper, solid-state reduction of nickel laterite was determined, the activation energies were calculated and the most probable mechanism function was determined by the Malek method.

Thermal Analysis Kinetics Theory

The activation energies were calculated usually by integral and differential methods. FWO method is the most commonly used integral method, besides, Starink method and KAS method are the most commonly used differential methods. The equation of FWO method is derived as

$$\lg \beta = \lg \left(\frac{AE}{RG(\alpha)} \right) - 2.315 - 0.4567 \frac{E}{RT} \quad (1)$$

The equation of Starink method is derived as

$$\ln \left(\frac{\beta}{T^{1.8}} \right) = \text{constant} - 1.0037 \frac{E}{RT} \quad (2)$$

The equation of KAS method is derived as

$$\ln \left(\frac{\beta}{T^2} \right) = \ln \frac{AR}{E} - \frac{E}{RT} \quad (3)$$

The most probable mechanism function was determined by the Malek method, and the Malek method is used to determine $f(\alpha)$ by $y(\alpha)$ which is defined.

$$y(\alpha) = \left(\frac{T}{T_{0.5}} \right)^2 \frac{\left(\frac{dz}{dt} \right)}{\left(\frac{dz}{dt} \right)_{0.5}} = \frac{f(\alpha) \cdot G(\alpha)}{f(0.5) \cdot G(0.5)} \quad (4)$$

In this paper, the most probable mechanism function was derived by the standard curve of $y(\alpha) - \alpha$. When the experimental curve and the standard curve coincide, the corresponding equation $f(\alpha)$ of the standard curve is the most probable mechanism function.

Experimental

The purity of carbon powder used in this experiment was 99.99% and the particle size was in 200–300 mesh.

Nickel laterite ore contains a large amount of water, with a moisture content on a dry basis of up to 50%, in the form of adsorbed and crystallised water [9]. The XRD experiments were carried out using D/max-3C (Co $K\alpha$) under the scanning rate of 4° min^{-1} . The XRD patterns shown in Fig. 1 reveals that the nickel laterite ores are typical saprolitic ore, containing dominant amounts of Mg silicate and Mg–Fe silicate minerals, and in nickel laterite ores, Ni occurs mainly in Mg silicates [10]. The XRD patterns shown in Fig. 2 reveals that the adsorbed and crystallised water mainly in $\text{CaAl}_2\text{Si}_2\text{O}_8(\text{H}_2\text{O})_4$ and hydroxyl groups mainly in $(\text{Mg}, \text{Al})_3(\text{Si}, \text{Fe})_2\text{O}_5(\text{OH})_4$ and $\text{Mg}_3\text{Si}_2\text{O}_5(\text{OH})_4$. Drying was performed at 1100°C in a corundum crucible within a muffle furnace for 2 h. Dried nickel laterite ores were ground to a 200 mesh-size using a laboratory-scale ball mill to mix with pure carbon powder to be homogeneous by a ratio of 1–1.2 used for TG and DTG analysis.

The chemical composition of nickel laterite ore was analysed by AAS method which is shown in Table 1.

The reduction behavior of the prepared samples was investigated using two different techniques, tg technique to measure the total weight loss of carbon and oxygen as a function of time and effluent gas analysis method for the outlet gases. The TG analysis was carried out using SetsysEvoTG-DTA1750 with three kinds of

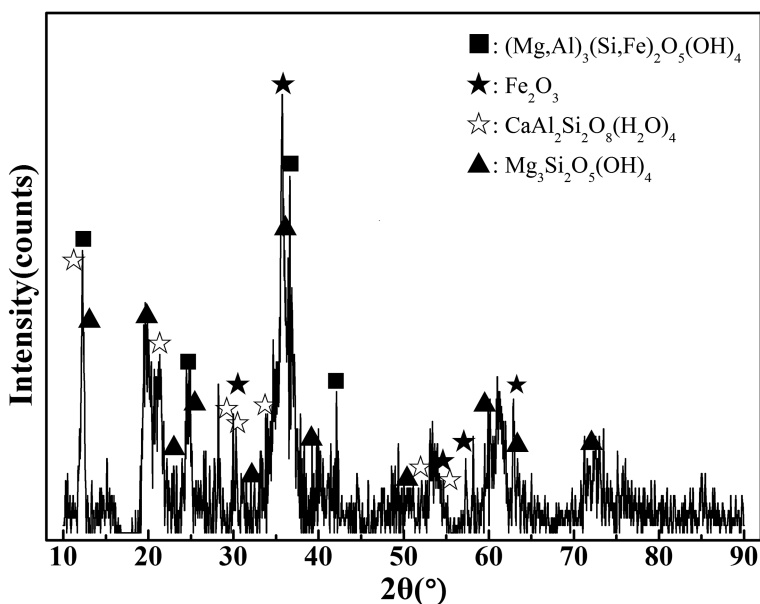


Fig. 1 X-ray diffraction pattern of nickel laterite

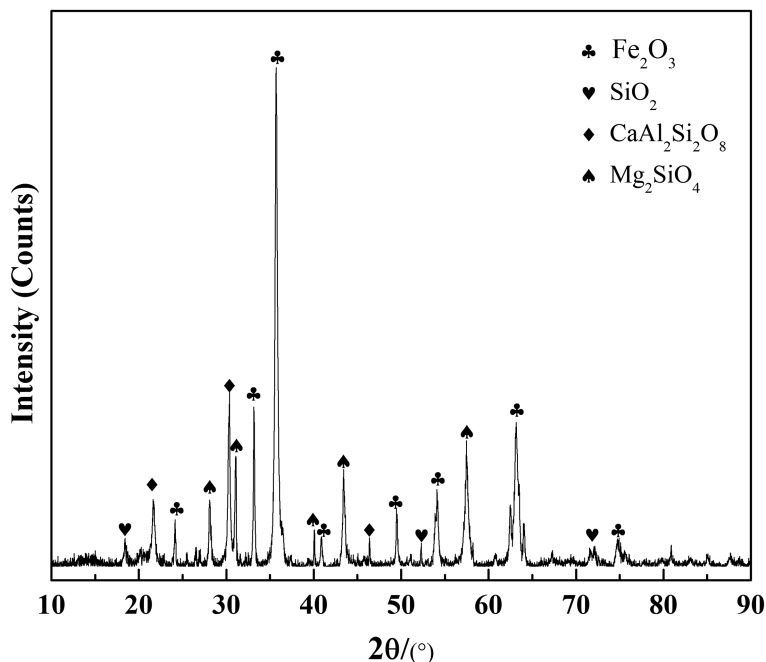


Fig. 2 X-ray diffraction pattern of nickel laterite at 1100 °C

Table 1 Chemical composition of nickel laterite/(wt%)

Ni	TFe	FeO	Cr ₂ O ₃	SiO ₂	Al ₂ O ₃	CaO	MgO	P	S
1.814	17.87	0.44	0.51	34.97	4.75	1.54	13.5	0.005	0.064

heating rate of 10 K/min, 15 K/min, 20 K/min under Ar atmosphere at a constant rate of 20 mL min⁻¹. The concentration of CO and CO₂ in the outlet gas were carried out using advanced quadrupole mass spectrometer (TILON LC-D200, AMETEK LLC., USA). Pure argon gas was passed over the compact at a constant rate of 20 mL min⁻¹. The degree of reduction and total weight loss of carbon and oxygen were calculated by the oxygen and carbon balance based on the CO and CO₂ concentrations obtained from gas analysis.

Results and Discussion

TG Analysis

TG was used to determine the thermal properties of nickel laterite ore, as shown in Fig. 3. It can be observed that weight loss is greatly affected by reduction

temperature. Increasing reduction temperature from 700 to 1400 °C causes the increase of the mass loss. In the initial stages of reduction, weight loss rate is slow, then the rate speeds up gradually and reach the maximum at about 1232 °C which can be seen clearly from DTG curves in Fig. 4, until 1400 °C, the process of reduction comes to an end, the weight of nickel laterite no longer changes. Besides, the heating speed has little influence on the weight loss ratio of nickel laterite ores.

Activation Energy Results and Discussion

The reduction fraction (α) of reduction of nickel laterite is defined as

$$\alpha = \frac{m_0 - m_t}{m_0 - m_\infty} \times 100\% \quad (5)$$

where, m_0 is the initial mass of sample, m_t represents the mass of the sample at arbitrary time t , m_∞ is the mass of the sample at the end of the process. The reaction fraction and DTG curves as a function of reduction temperature are shown in Fig. 4, in which the solid lines express the DTG curves while the dotted lines express the reaction fraction curves, in which, the reduction degree has no significant change as the reduction temperature increased, besides, the reduction rate is the highest at early stages ($\alpha = 0.3$).

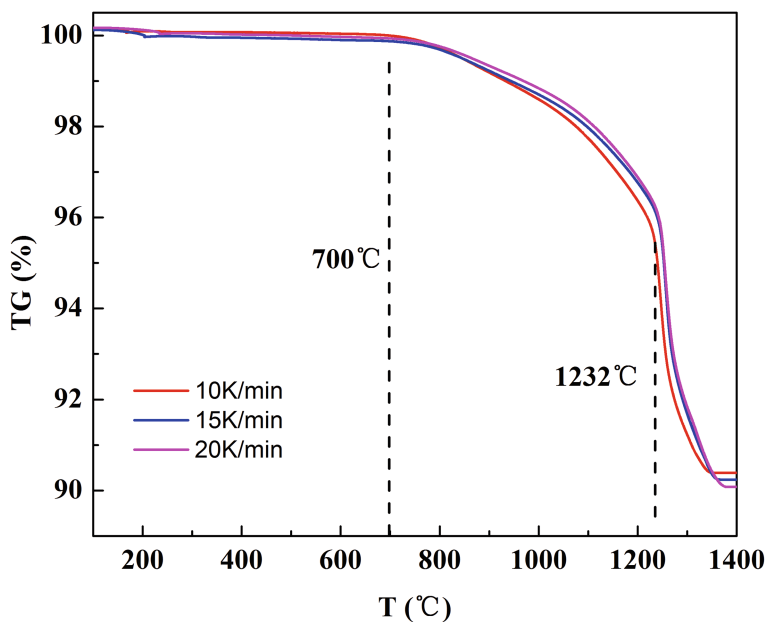


Fig. 3 TG curves of nickel laterite ore-carbon mixture at three heating rates

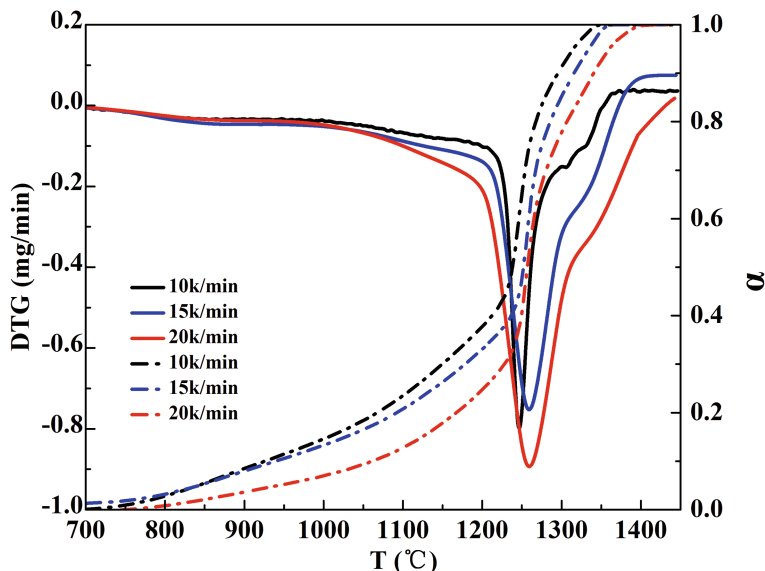


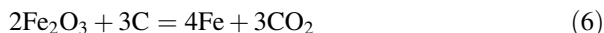
Fig. 4 Conversion fraction and DTG-temperature curves of nickel laterite ore-carbon mixture

The E values were determined by FWO method, Starink method and KAS method are shown in Fig. 5 and Table 2.

The reduction process is divided into three parts according to the E values, besides, the temperature corresponding to the three parts is shown in Fig. 5. In the range of $0.10 \leq \alpha \leq 0.40$ and $0.70 \leq \alpha \leq 0.90$, the activation energies are the constant value. Until for $0.40 \leq \alpha \leq 0.70$, the E values have a great change, the values increased with increasing α values.

The obtained activation energy is in good agreement with E values which were determined by Malek et al. [11] and Liao et al. [12], respectively. According to the research of Vyazovkin [13], if the activation energy is independent on α values, the reaction is single-step reaction, however, the reaction is multi-step reaction if the activation energy varies with the change of α values. From Fig. 5, in the wide range of $0.10 \leq \alpha \leq 0.40$ and $0.70 \leq \alpha \leq 0.90$, the proof of existing of single-step reaction is evident, however, in the range of $0.40 \leq \alpha \leq 0.70$ designated on the existence of parallel independent reaction.

In this study, the possible reactions are as follows,



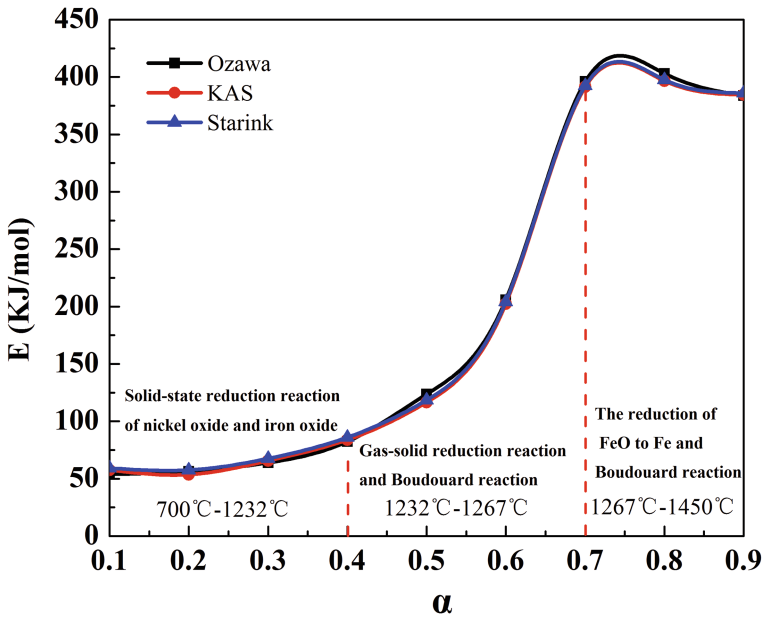
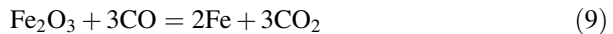


Fig. 5 Relationship between conversion fraction and activation energies

Table 2 Calculated activation energies through different methods

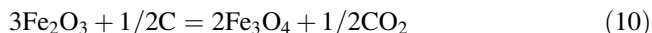
α	$E\alpha$ /(KJ/mol)		
	FWO	Starink	KAS
0.10	53.93	57.47	59.28
0.20	56.31	53.49	57.50
0.30	63.94	65.56	67.58
0.40	82.26	83.95	86.00
0.50	123.79	116.55	118.53
0.60	205.92	202.37	204.09
0.70	396.20	391.38	392.46
0.80	403.01	396.61	397.71
0.90	383.95	384.59	386.03



It is reported that NiO was firstly reduced, and then the metallic Ni could use metallic Fe as the carriers to form Fe–Ni alloy to separate from the gangue minerals [14]. At the beginning of the reduction process, the nickel laterite powders and pure carbon powders are close to each other, the preferential reduction of nickel oxide to metallic nickel can occur as Eq. (7), and the reduction of iron oxide to metallic iron takes place as Eq. (6). Then, the reaction between iron oxides and carbon monoxide generated by Boudouard reaction takes place as Eq. (9).

It is well known that the reduction reactions of iron oxides proceed in a stepwise manner ($\text{Fe}_2\text{O}_3\text{-Fe}_3\text{O}_4\text{-FeO-Fe}$). To detect the reduction situation of iron oxides in nickel laterite, XRD were used to study the reduction product at 1000, 1250, 1300 and 1400 °C which is shown in Fig. 6.

In the range of $0.10 \leq \alpha \leq 0.40$, the reduction reaction has a low activation energy and a fast speed, and Fig. 6 shows that the reduction product of iron oxides is Fe_3O_4 , this suggests that Fe_2O_3 is mainly reduced into Fe_3O_4 by carbon, the possible reaction is listed as follows,



In the unreacted-core shrinking model shown in Fig. 7a, the nickel laterite powders and pure carbon powders are close to each other in the initial stage, then the oxygen of Fe_2O_3 are removed to generate Fe_3O_4 particle and CO_2 .

The connection of the rate-controlling step of reduction rate to the activation energy of iron oxide was investigated by Nasr [15] (Table 3). In this stage, the E values are almost within 55–67 kJ/mol, hence, the rate-controlling step in this stage is performed as inner chemical reaction.

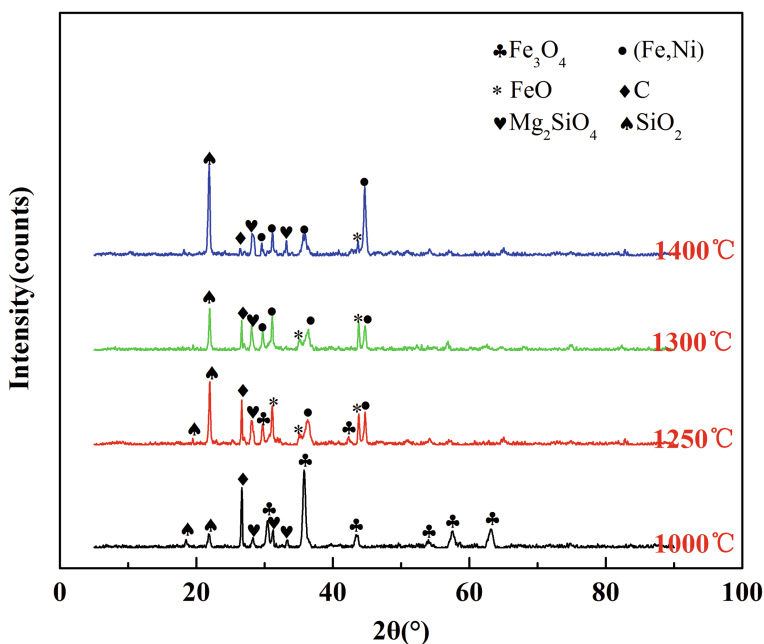


Fig. 6 X-ray diffraction pattern of nickel laterite ore-carbon mixture at 1000, 1250, 1300 and 1400 °C

Fig. 7 Unreacted-core shrinking model for Fe_2O_3 reduction

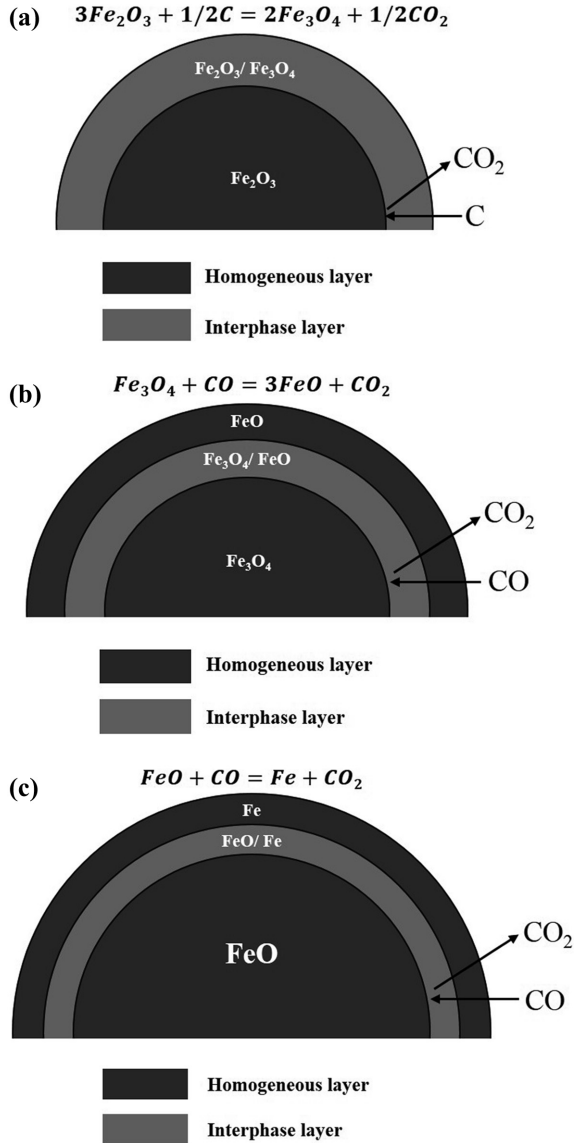
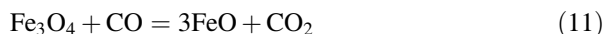


Table 3 Relationship of rate-controlling step and activation energy of iron oxide

$E/(kJ/mol)$	Rate-controlling step
8–16	Inner gas diffusion
29–42	Inner gas diffusion and interface chemical reaction mixed
55–67	Interface chemical reaction
>80	Solid diffusion

In the range of $0.40 \leq \alpha \leq 0.70$, Fig. 6 shows that the reduction product of iron oxides are mostly FeO and a small part of Fe–Ni, this suggests that Fe₃O₄ is reduced into FeO and Fe–Ni, the possible reactions are listed as follows,



As Fig. 7b shows that CO diffuses across the FeO layer to reach the Fe₃O₄–FeO interphase layer, and CO reacts with Fe₃O₄ to generate CO₂. In this stage, the *E* values have a great change, the *E* values increased with increasing α values. In the initial stage ($\alpha = 0.4$), the *E* values are almost 80 kJ/mol, hence, the rate-controlling step is performed as solid diffusion according to the study of Nasr [15].

In the range of $0.70 \leq \alpha \leq 0.90$, Fig. 6 shows that the reduction products of iron oxides are mostly Fe–Ni and a small part of FeO at 1300 °C and iron oxides are all reduced into Fe–Ni at 1400 °C, the possible reaction is given as follows,



As Fig. 7c shows that CO diffuses across the Fe layer to reach the FeO–Fe interphase layer, and CO reacts with FeO to generate CO₂.

In the range of 1100–1350 °C, the variation of CO and CO₂ in the outlet gas is shown in Fig. 8. It can be observed that the rate of formation of CO₂ is greater than that of CO particularly in the range of $0.50 \leq \alpha \leq 0.90$ and then slows down. It is reasonable to accept that Boudouard reaction is the major controlling step in this stage.

Model Function Results

Based on the Malek analysis, the standard curves were first obtained for the forty-one model functions. Figures 9, 10 and 11 show that the experimental data points are both almost have the same trend.

In the range of $0.10 \leq \alpha \leq 0.40$, the mechanism function is chemical reaction order function (No. 37) shown as follows:

$$f(\alpha) = (1 - \alpha)^{-1} - 1 \quad (13)$$

$$G(\alpha) = (1 - \alpha)^2 \quad (14)$$

In the range of $0.40 \leq \alpha \leq 0.70$ and $0.70 \leq \alpha \leq 0.90$, the shapes of the experimental curves vary somewhat with the standard curves, this indicates that the mechanism of the process under investigation may not be exactly described by one mechanism function.

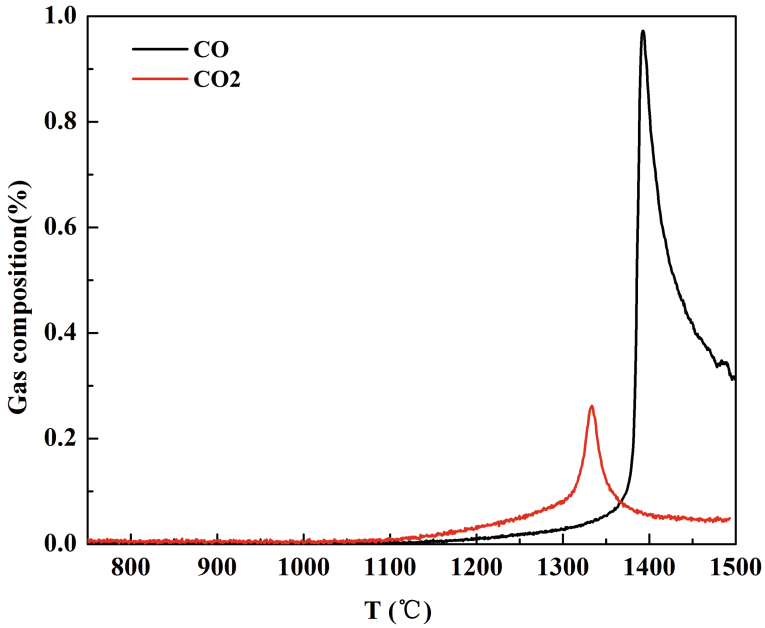


Fig. 8 Variation of gas composition (CO and CO₂) as a function of temperature

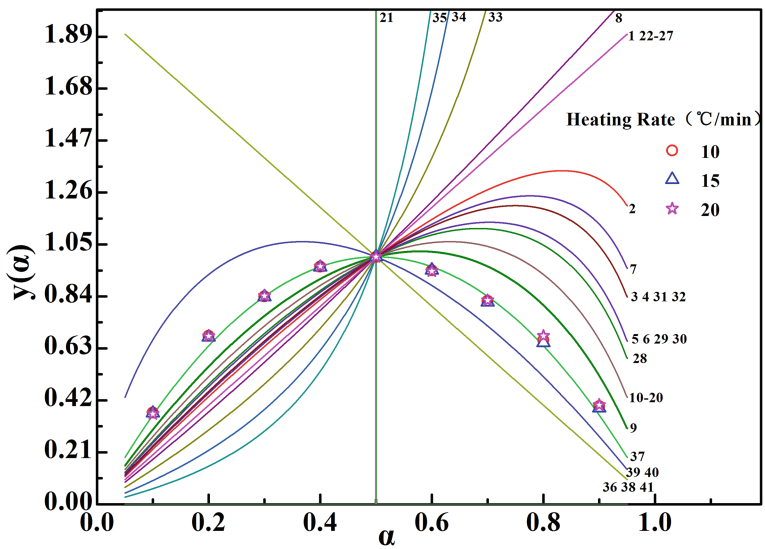


Fig. 9 The standard $y(\alpha)$ - α curves and the actual $y(\alpha)$ - α curves of solid-state reduction in the range of $0.10 \leq \alpha \leq 0.40$

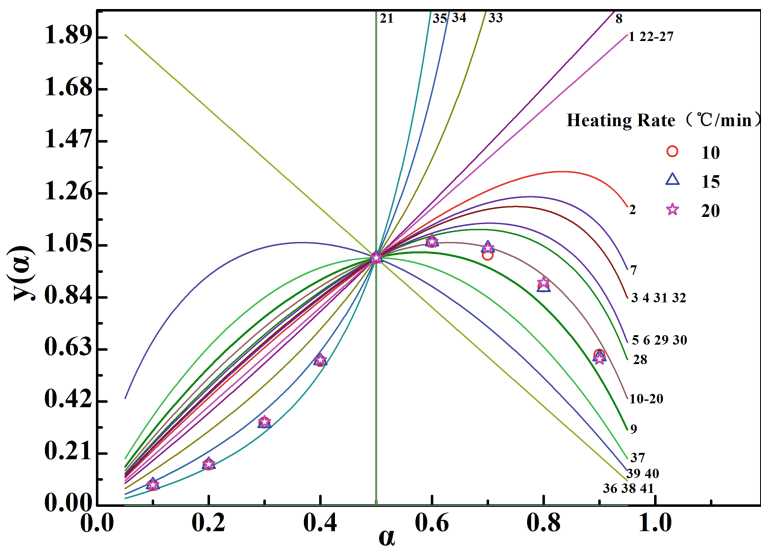


Fig. 10 The standard $y(\alpha)$ - α curves and the actual $y(\alpha)$ - α curves of solid-state reduction in the range of $0.40 \leq \alpha \leq 0.70$

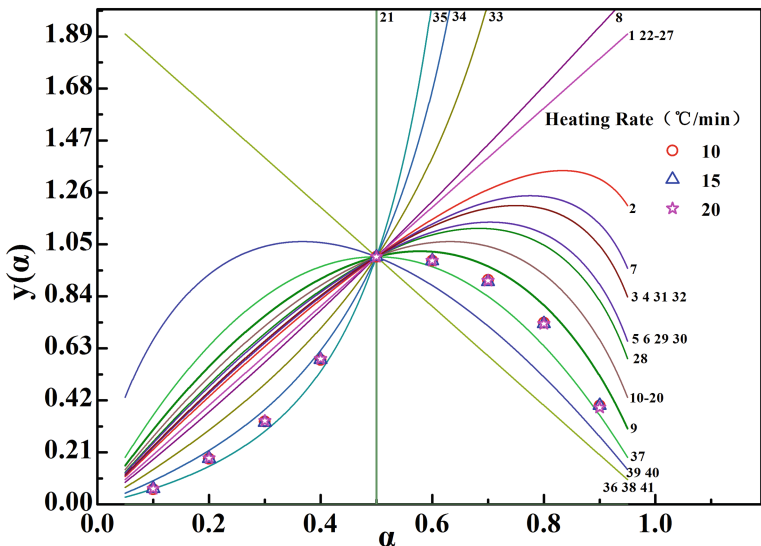


Fig. 11 The standard $y(\alpha)$ - α curves and the actual $y(\alpha)$ - α curves of solid-state reduction in the range of $0.70 \leq \alpha \leq 0.90$

Conclusions

- (1) The weight loss ratio of nickel laterite ores is mainly related to the heating temperature; the heating speed has little influence.
- (2) In the range of $0.10 \leq \alpha \leq 0.40$, the average E values are 59.45 kJ/mol. In the range of $0.40 \leq \alpha \leq 0.70$, the average E values are 136.77 kJ/mol and in the range of $0.70 \leq \alpha \leq 0.90$, the average E values are 383.95 kJ/mol.
- (3) In the range of $0.10 \leq \alpha \leq 0.40$, solid-state reduction reaction of nickel oxide and iron oxide of Fe_2O_3 to Fe_3O_4 mainly happened. In the range of $0.40 \leq \alpha \leq 0.70$, gas-solid reduction reaction of Fe_3O_4 to FeO and Boudouard reaction mainly happened. In the range of $0.70 \leq \alpha \leq 0.90$, the reduction reaction of FeO to Fe and Boudouard reaction mainly happened.
- (4) In the range of $0.10 \leq \alpha \leq 0.40$, the experimental data points are both targeting the chemical reaction order function. In the range of $0.40 \leq \alpha \leq 0.70$ and $0.70 \leq \alpha \leq 0.90$, the results showed that the process may not be exactly described by one mechanism function.

Acknowledgements The authors are especially grateful to The National Natural Science Foundation of China (No. 51234010).

References

1. X.M. Li et al., Technology of treating nickel-bearing laterite. *Ferro-Alloys* **4**, 24–28 (2007)
2. X.Y. Guo et al., The statue quo and prospect of the technologies of nickel laterites. *Metal. Mater. Metall. Eng.* **2**, 3–9 (2009)
3. J.B. Chen et al., Status quo of nickel mineral resource of our country and countermeasures. *Express Inf. Mining Ind.* **8**, 1–3 (2006)
4. Y.P. Zhang et al., Characteristics of laterite resource and analysis on its pyrometallurgy process. *Ferro-Alloys* **6**, 18–21 (2007)
5. S.W. Zhang, Status quo of nickel resources, production and consumption. *World Nonferrous Metals* **8**, 9–14 (2006)
6. B. Jankovic, B. Adnadevic, S. Mentus, The kinetic analysis of non-isothermal nickel oxide reduction in hydrogen atmosphere using the invariant kinetics parameters method. *Thermochim. Acta* **456**, 48–55 (2007)
7. B. Jankovic, B. Adnadevic, S. Mentus, The kinetic study of temperature-programmed reduction of nickel oxide in hydrogen atmosphere. *Chem. Eng. Sci.* **63**, 567–575 (2008)
8. J. Kim, G. Dodibiba, H. Tanno, Calcination of low-grade laterite for concentration of Ni by magnetic separation. *Miner. Eng.* **23**, 282–288 (2010)
9. D.A. Silva et al., Thermodynamic aspects of the roasting processes in the pre-treatment of nickelferrous garnierites. *Mineral Process. Extr. Rev. Int. J.* **9**, 97–104 (1992)
10. P. Wu et al., Prediction of the thermodynamic properties and phase diagrams of silicate systems-evaluation of the FeO-MgO-SiO₂ system. *Trans. Iron Steel Inst. Jpn.* **33**, 26–35 (1993)
11. J.M. Criado et al., Application of the master plots in kinetic analysis of non-isothermal data. *Thermochim. Acta* **147**, 377–385 (1989)

12. J.L. Liao et al., Influence of TiO_2 and basicity on viscosity of Ti bearing slag. *Ironmaking Steelmaking* **39**, 133–139 (2013)
13. S. Vyazovkin et al., An approach to the solution of the inverse kinetic problem in the case of complex process. Part III. Parallel independent reactions. *Thermochim. Acta* **197**, 41–51 (1992)
14. Y. Zhang et al., Reduction of Fe and Ni in Fe-Ni-O systems. *J. Min. Metall.* **49**, 13–20 (2013)
15. M.I. Nasr et al., Effect of nickel oxide doping on the kinetics and mechanism of iron oxide reduction. *Trans. Iron Steel Inst. Jpn.* **35**, 1043 (1995)